# I. APPENDIX

**What VRA Guarantees**. VRA provides a step-wise realizability contract at the actuator current level. At each discrete step $k$ , VRA constructs an admissible q-axis current interval $\mathcal{I}_k$ from the voltage constraint. Any executed command is obtained by projecting onto $\mathcal{I}_k$, hence it admits an actuator realization that respects the voltage limit under the stated model assumptions (Lemma 1). VRA does not provide trajectory-level invariance, viability, or safety guarantees. It only ensures that kinematically admissible accelerations are not silently unrealizable due to voltage limits.

This appendix provides additional derivations and implementation details omitted from the main paper due to space constraints, with the goal of improving technical clarity and reproducibility. We offer an open-source project [1], including the MATLAB Simulink model of VRA, the commonly used joint-level kinematic envelop VBAC, the USB2FDCAN communication driver, and the actuator driver used in experiments.

## A. Motor Physics

We briefly restate the actuator model from the main paper to keep this appendix self-contained. Permanent-magnet synchronous motors (PMSMs) are widely used in robotic systems [2, 1, 6]. Both surface-mounted (SPMSM) and interior (IPMSM) PMSMs are subject to a current-limit ellipse (CLE) and a voltage-limit ellipse (VLE) [5], as illustrated in Fig. A1. The VLE is velocity dependent, reflecting the fact that the available voltage budget constrains achievable torque as joint speed increases. For a fixed $i_d$, the intersection of the constant-torque line (CTL) with the VLE defines the maximum feasible torque at that speed. When the torque required to realize a commanded joint acceleration exceeds this limit, the command becomes physically unrealizable due to the voltage constraint. Therefore, the proposed method does not address PMSM control itself, but instead proposes a contract between kinematic reasoning and actuator physics.

## B. Implementation Details

For notation brevity we write $S_{\text{tr},k}(\dot{q}_k)$ and $S_{\text{st},k}(\dot{q}_k)$, but both sets are computed online from the measured state and input history (e.g., $\dot{q}_{k-2}$, $i_{q,k-1}$, and $\boldsymbol{u}_{k-1}$). Thus, they are not purely functions of $\dot{q}_k$ and computed through (12a)-(12i) in the main paper.

*1) Admissible Current Set:* The set of admissible $q$ axis current is the intersection of $\mathcal{S}_{\text{tr}}(\dot{q}_k)$ and $\mathcal{S}_{\text{st}}(\dot{q}_k)$. $\mathcal{S}_{\text{tr}}(\dot{q}_k)$ is the instantaneous feasibility of the current, and it's tuning-free. $\mathcal{S}_{\text{st}}(\dot{q}_k)$ provides a look-ahead constraint that anticipates near-future back-EMF effects, and explicitly depends on $M$ and $s$.

To construct a practical $\mathcal{S}_{\text{st}}(\dot{q}_k)$, we account for three considerations. (i) **External actuator loads.** In general, (12g) should include the external load torque:

$$\hat{u}^{\text{st}}_{q,k} := i_{q,k}R_s + \left(\dot{q}_{k-1} + \frac{k_t i_{q,k} - \tau_{\text{load}}}{M}\, s\Delta t\right) p\varphi + u^{\text{res}}_{q,k}, \quad \text{(A1)}$$

[1] **https://github.com/jointlevelVRA/VRA_Drivers**

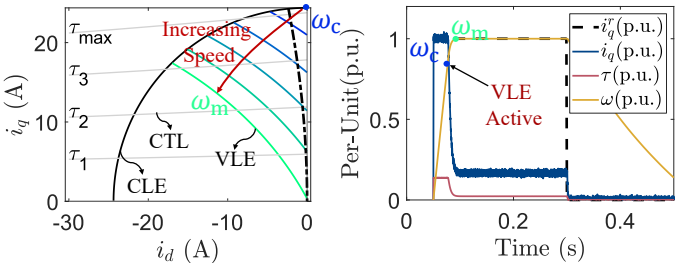


Fig. A1: **PMSM constraints.** (Right) The operating region of PMSM-based actuators is bounded by the current-limit ellipse (CLE) and the speed-dependent voltage-limit ellipse (VLE). For a fixed $i_d$, the intersection of the constant-torque line (CTL) with the VLE determines the maximum achievable torque at a given speed. (Left) If a commanded acceleration requires torque beyond this VLE-imposed limit, the realized torque is distorted once the VLE becomes active (illustrated by the per-unit traces). $\omega_c$ denotes the corner speed, $\omega_m$ the maximum speed under $i_d = 0$, and p.u. denotes per-unit.

where $\tau_{\text{load}}$ denotes the net external torque acting on the actuator. In this work, we deliberately neglect $\tau_{\text{load}}$, since the exact contact sequence and external forces of legged robots are generally difficult to estimate reliably online. Many approaches assume a predefined gait [4, 3] and model only gravity and centrifugal terms, treating the remaining interaction forces as disturbances. Following this practice, we drop $\tau_{\text{load}}$ and absorb its effect into unmodeled disturbances.

**Remark A1 (Effect of External Loads and Impacts)**. The admissible current set $\mathcal{I}_k$ is derived without explicitly modeling external load torques. In implementation, moderate unmodeled effects are treated as residual voltage terms and compensated step-wise. VRA is intended to remain valid as long as these disturbances do not drive the actuator outside the assumed voltage-feasible operating regime. We do not claim formal robustness guarantees, and this remark only clarifies how moderate disturbances enter the residual voltage compensation in practice.

(ii) **Look-ahead step $s$.** We introduce a look-ahead step to account for non-negligible latency between command issuance and feedback availability. Such delays can cause unrealizability on hardware even when the algorithm, operating on delayed measurements, predicts feasibility. The latency depends on the communication stack (e.g., EtherCAT at the $\mu$s scale versus SPI-CAN [2] at the ms scale). In our system, the communication delay is 3–4 ms, and we therefore choose $s = 10$ steps.

**Remark A2 (Interpretation of the Look-Ahead Parameter $s$).** The parameter $s$ is a tunable anticipation hyperparameter (not a physical inertia) that encodes a conservative look-ahead horizon for voltage feasibility under discretization mismatch and command/feedback latency. Practically, $s$ is chosen to exceed the measured delay so that $\mathcal{S}_{\text{st}}$ constrains near-future back-EMF demand, reducing saturation and switching-prone behavior near kinematic boundaries. The look-ahead step $s$ is defined in *execution* steps, i.e., the look-ahead window is $s\Delta t$ (not $s\Delta t_p$), and we choose $s\Delta t$ to exceed the measured command-to-feedback delay.

(iii) **Inertial hyperparameter.** Accurate inertia identifica-

TABLE A3: Fitted MOR boundary from dynamometer data at 48 V.

| Parameter | 8115 (48V) | 6210 (48V) | Unit |
|---|---|---|---|
| Boundary model | $\tau^{48}_{\max}(\dot{q}) = a_{48}\dot{q} + b_{48}$ | same | – |
| $a_{48}$ | $-4.5622$ | $-2.1749$ | N·m·s/rad |
| $b_{48}$ | 125.1373 | 74.92 | N·m |
| $R^2$ | 0.9944 | 0.9901 | – |

tion is challenging in practice, and the effective inertia can vary across maneuvers. Since $M$ strongly influences $\mathcal{S}_{\text{st}}(\dot{q}_k)$, we introduce a tunable gain $z$ and use $Mz$ as an effective constant mapping from torque to acceleration. The parameter $z$ is tuned to match the empirically observed torque limit when $s = 1$. With these considerations, we implement (12g) as:

$$\hat{u}^{\text{st}}_{q,k} := i_{q,k}R_s + \Big(\dot{q}_{k-1} + \frac{k_t i_{q,k}}{Mz}\, s\Delta t\Big)p\varphi + u^{\text{res}}_{q,k}. \quad \text{(A2)}$$

Note that this gain only affects the conservatism of the acceleration bound, not the voltage feasibility that defines $\mathcal{I}_k$. The "empirically observed torque limit" refers to the maximum realized torque under step-torque tests before sustained VLE activation (same motor/drive setting as Table A2), and $z$ is fixed thereafter across all trials for that motor.

*2) Voltage Bus and Voltage Budget:* The DC bus voltage $V_{\text{bus}}$ is the power-supply voltage of the robotic system, while the voltage budget $V_{\text{limit}}$ is the constant voltage constraint used in VRA. Under SVPWM (without over-modulation), they are related by

$$V_{\text{limit}} = \alpha \frac{V_{\text{bus}}}{\sqrt{3}} \quad \text{(A3)}$$

Here $\alpha$ is a tunable hyperparameter that adjusts the voltage-based velocity limit encoded in (11).

With the admissible current set $\mathcal{I}_k$ and the voltage budget $V_{\text{limit}}$ specified above, we present VRA in Algorithm A1, which computes the voltage-feasible acceleration set at each step and projects the commanded acceleration onto this set for execution.

**Remark A3 (When VRA Adds Conservatism).** When the voltage budget is sufficient, the voltage-feasible set $\mathcal{I}_k$ contains the nominal acceleration demand, so VRA recovers the original kinematic envelope and introduces no extra restriction. Additional conservatism appears only near voltage-limited regimes, where VRA intentionally tightens admissible accelerations to avoid kinematically admissible but physically unrealizable commands.

### C. Experimental Details

For the first experiment, we evaluate the proposed method on two SPMSM actuators (Fig. A2) under multiple operating conditions, and the corresponding motor parameters are listed in Table A2. For all subsequent experiments, we use the 8115 motor, including validation on a quadruped wheel-legged robot equipped with the same 8115 actuators.

*1) Acceleration Bounds from Voltage Constraints:* **Constructing MOR**. Following [7], the motor operating region (MOR) is defined as a speed-dependent linear torque boundary

$$\tau^{\text{ub}}(\dot{q}) = a_{48}\dot{q} + b_{48}, \quad \text{(A4)}$$

**Algorithm A1** Proposed VRA

**Require:** motor state $x_{k-1} = (q_{k-1}, \dot{q}_{k-1})$, raw acceleration command $\ddot{q}^{\text{r}}_k$, sampled feedback $i_{q,k-1}, \boldsymbol{u}_{k-1}$, motor parameters, joint position bound $q^{\text{ub}}$, execution step $\Delta t$, kinematic envelope step $\Delta t_p$, look-ahead step $s$

**Ensure:** realizable $\ddot{q}_k$

$\dot{q}_k \leftarrow \dot{q}_{k-1}$ *Assumption 1*

$\boldsymbol{u}^{\text{n}}_{k-1} \leftarrow \text{NominalVoltage}(\dot{q}_{k-1}, i_{q,k-1})$ *(12a)(12b)*

$\boldsymbol{u}^{\text{res}}_k \leftarrow \boldsymbol{u}^{\text{n}}_{k-1} - \boldsymbol{u}_{k-1}$ *Assumption 2*

$\mathcal{S}_{\text{st},k} \leftarrow \text{ComputSet}_{\text{tr}}(\boldsymbol{u}^{\text{res}}_k, \dot{q}_{k-1}, i_{q,k-1}, \Delta t, s)$ *(12f)*

$\mathcal{S}_{\text{tr},k} \leftarrow \text{ComputeSet}_{\text{st}}\ (\boldsymbol{u}^{\text{res}}_k, \dot{q}_{k-1}, \Delta t)$ *(12g)*

$\mathcal{I}_k = \mathcal{S}_{\text{st}} \cap \mathcal{S}_{\text{tr}}$

$[\ddot{q}^{\text{lb}}_k, \ddot{q}^{\text{ub}}_k] \leftarrow \text{NominalDynamics}(\{i_{q,k}, i_{q,k} \in \mathcal{I}_k\})$ *(12k)*

$\ddot{q}^{\max}_k \leftarrow \text{SelectBrakingLimits}(\dot{q}_{k-1}, \ddot{q}^{\text{lb}}_k, \ddot{q}^{\text{ub}}_k)$ *(13a)(13b)*

$[\ddot{q}^{\text{lb}}_{\text{p},k}, \ddot{q}^{\text{ub}}_{\text{p},k}] \leftarrow \text{KinematicEnvelop}(\Delta t_p, q^{\max}, \ddot{q}^{\max}_k)$

$\ddot{q}_{\text{p},k} \leftarrow \text{Clamp}(\ddot{q}^{\text{lb}}_{\text{p},k}, \ddot{q}^{\text{ub}}_{\text{p},k}, \ddot{q}^{\text{r}}_k)$

$\ddot{q}_k \leftarrow \text{Clamp}(\ddot{q}^{\text{lb}}_k, \ddot{q}^{\text{ub}}_k, \ddot{q}_{\text{p},k})$

**return** $\ddot{q}_k$

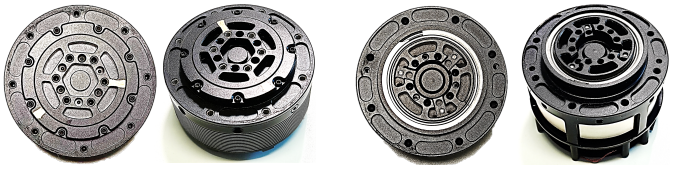

(a) Motor 8115 (b) Motor 6210

Fig. A2: **Motors used in the experiments**. The two motors have similar ratings but different inertia and pole-pair configurations, allowing evaluation across distinct actuator characteristics.

TABLE A2: Motor parameters and low-level drive settings used in experiments.

| Symbol | Motor 8115 | Motor 6210 | Unit | Source |
|---|---|---|---|---|
| Flux linkage $\varphi$ | 0.005357 | 0.005257 | $Wb$ | Measured |
| Phase Inductance $L_s$ | 0.000105 | 0.000109 | $H$ | Measured |
| Phase Resistor $R_s$ | 0.1625 | 0.14237 | $\Omega$ | Measured |
| Pole pairs $N_p$ | 21 | 14 | - | Datasheet |
| Torque limit $\tau_{max}$ | 35 | 25 | $N \cdot m$ | Identified |
| Inertia $J$ | 0.007 | 0.003 | $kg \cdot m^2$ | Identified |
| Motor Diameter $D$ | 95 | 75 | $mm$ | Measured |
| Gear ratio $G_r$ | 9.75 | 10.75 | - | Config |
| *Low-level drive and control* | | | | |
| Current control | FOC ($dq$-PI) | same | – | Config |
| PWM frequency $f_{\text{sw}}$ | 80 | same | $kHz$ | Config |
| Cuurent-control period $T_i$ | 25 | same | $\mu s$ | Config |
| Current-loop bandwidth $f_i$ | 1100 | same | $Hz$ | Identified |
| Current limit $I_{\max}$ | 40 | same | $A$ | Config |
| Bus voltage $V_{\text{bus}}$ | 19-48 | same | $V$ | Config |
| Cmd update rate $f_{\text{cmd}}$ | 1000 | same | $Hz$ | Config |
| Fb Sampling period $\Delta t$ | 0.001 | same | $s$ | Config |
| Cmd-fb delay $T_d$ | 4 | same | $ms$ | Measured |

The current-loop bandwidth is the closed-loop $-3$db cutoff of $i^*_q \to i_q$. The command-to-feedback delay includes $q, \dot{q}, i_q$. The two motors are shown in Fig. A2

where $a_{48}$ and $b_{48}$ are identified from dynamometer measurements collected at a 48 V voltage (See Table A3). Because our experiments run at lower bus voltages, we scale the MOR boundary according to the available voltage budget, using the same budget definition as (A3). This scaling preserves the original MOR shape while accounting for reduced voltage headroom, and represents a best-effort adaptation of MOR under varying bus voltages. We then linearly scale the MOR

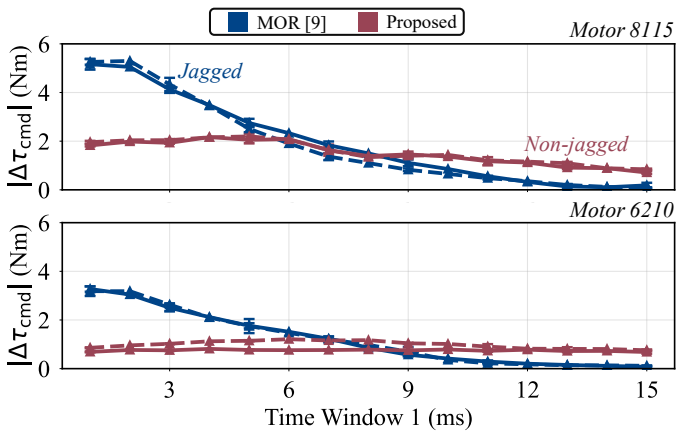


(a) Slew rate of acceleration realization.

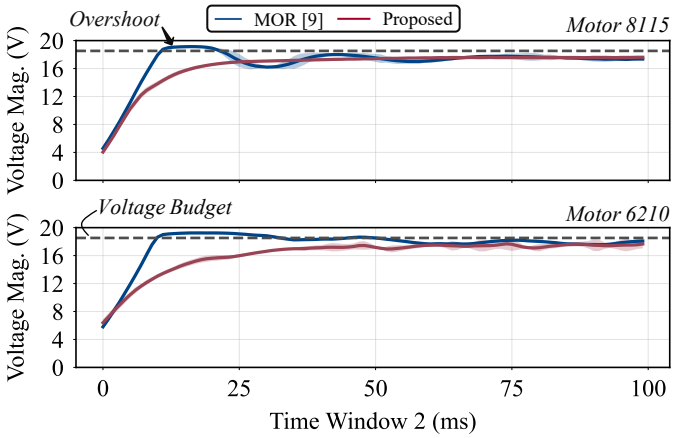


(b) Voltage magnitude.

Fig. A3: **Underlying reason why VRA improve acceleration feasibility**. (a) Acceleration realization slew rate over a short window: MOR exhibits jagged, switching-prone behavior, while the proposed method remains non-jagged. (b) Corresponding voltage magnitude trajectories over a longer window: MOR frequently produces voltage overshoot beyond the available voltage budget, whereas the proposed method stays within the budget with reduced saturation risk.

intercept term as

$$b_v = b_{48}\frac{\alpha V_{\text{bus}}}{48}. \tag{A5}$$

Thus, for 24 V and 36 V experiments, $b_{24} = 0.45b_{48}$ and $b_{36} = 0.675b_{48}$. Concretely, for 8115 motor, $b_{24} = 56.31$ Nm and $b_{36} = 84.48$ Nm; for the 6210 motor, $b_{24} = 32.36$ Nm and $b_{36} = 48.55$ Nm.

**Underlying Reason of Improved Feasibility**. To quantify saturation-induced torque distortion, we analyze two time windows around the step input. The Time Window 1 lasts 15 ms, and denotes the first instant when $\ddot{q}_k$ reaches the boundary. We report (i) the fraction of control samples for which the low-level saturation flag is active and (ii) the torque-command slew rate over the same interval. In addition, under the stressed condition (36 V/45 °C), we examine the first 100 ms after the step onset by computing the applied voltage magnitude $\|\boldsymbol{u}_k\|$, denoted with Time Window 2, and comparing it with the voltage budget $V_{\text{limit}}$, which characterizes both the feasibility and the smoothness of the voltage trajectory.

Although MOR and VRA can both appear to "clip" infeasible commands at execution time, they differ fundamentally in design intent and in what is being constrained. As shown in Fig. A3, MOR enforces feasibility by post-hoc torque clipping against fixed, sampled boundaries, which can be inaccurate under changing conditions. This often yields switching-prone, jagged torque adjustments near the limit and can manifest as transient voltage overshoot and saturation. In contrast, VRA is formulated as an execution-level realizability interface that exposes a state-dependent, voltage-feasible acceleration set to upstream kinematic reasoning. Any residual projection at runtime is only a practical safeguard against model mismatch, and the resulting torque shaping and voltage trajectories remain smooth and within the available voltage budget.

*2) Kinematic Envelope:* **Deceleration Bounds**. In Experiment 2, the aggressive bound (AB) refers to the min–max constant acceleration limits used in VBAC and the corresponding realized torque, while the conservative bound (CB) refers to the nominal constant acceleration limits and the corresponding realized torque. On Motor 8115, AB and CB correspond to realized torques of 30 Nm and 20 Nm, respectively. These two settings are used to represent the constant braking limits in VBAC.

**Interpretation of Failure Modes**. In Table II, failures fall into two categories. (i) *Hardware protection*: the actuator driver (DRV8353) triggers fault protection (e.g., over-current or over-voltage), which terminates execution when infeasible acceleration commands are issued. (ii) *Unrealized acceleration commands*: when the commanded realized torque deviates substantially from the measured torque, the kinematic execution becomes invalid, and the trial is marked as a failure. In our tests, the run with $\Delta t_p = 0.001\ s$ fails due to hardware protection, whereas the run with $\Delta t_p = 0.005\ s$ fails due to unrealized commanded accelerations.

## References


[1] Marco Hutter, Christian Gehring, Dominic Jud, Andreas Lauber, C. Dario Bellicoso, Vassilios Tsounis, Jemin Hwangbo, Karen Bodie, Peter Fankhauser, Michael Bloesch, Remo Diethelm, Samuel Bachmann, Amir Melzer, and Mark Hoepflinger. Anymal - a highly mobile and dynamic quadrupedal robot. In *2016 IEEE/RSJ International Conference on Intelligent Robots and Systems (IROS)*, pages 38–44, 2016. doi: 10.1109/IROS.2016.7758092.

[2] Benjamin Katz, Jared Di Carlo, and Sangbae Kim. Mini cheetah: A platform for pushing the limits of dynamic quadruped control. In *2019 International Conference on Robotics and Automation (ICRA)*, pages 6295–6301, 2019. doi: 10.1109/ICRA.2019.8793865.

[3] Gijeong Kim, Dongyun Kang, Joon-Ha Kim, Seungwoo Hong, and Hae-Won Park. Contact-implicit model predictive control: Controlling diverse quadruped mo-

tions without pre-planned contact modes or trajectories. *The International Journal of Robotics Research*, 44(3):486–510, October 2024. ISSN 1741-3176. doi: 10.1177/02783649241273645. URL http://dx.doi.org/10.1177/02783649241273645.

[4] Junheng Li, Ziwei Duan, Junchao Ma, and Quan Nguyen. Gait-net-augmented implicit kino-dynamic mpc for dynamic variable-frequency humanoid locomotion over discrete terrains, 2025. URL https://arxiv.org/abs/2502.02934.

[5] S. Morimoto, Y. Takeda, T. Hirasa, and K. Taniguchi. Expansion of operating limits for permanent magnet motor by current vector control considering inverter capacity. *IEEE Transactions on Industry Applications*, 26(5):866–871, 1990. doi: 10.1109/28.60058.

[6] Young-Ha Shin, Seungwoo Hong, Sangyoung Woo, JongHun Choe, Harim Son, Gijeong Kim, Joon-Ha Kim, KangKyu Lee, Jemin Hwangbo, and Hae-Won Park. Design of kaist hound, a quadruped robot platform for fast and efficient locomotion with mixed-integer nonlinear optimization of a gear train. In *2022 International Conference on Robotics and Automation (ICRA)*, pages 6614–6620, 2022. doi: 10.1109/ICRA46639.2022.9811755.

[7] Young-Ha Shin, Tae-Gyu Song, Gwanghyeon Ji, and Hae-Won Park. Reinforcement learning for high-speed quadrupedal locomotion with motor operating region constraints: Mitigating motor model discrepancies through torque clipping in realistic motor operating region. *IEEE Robotics Automation Magazine*, 32(2):49–59, 2025. doi: 10.1109/MRA.2024.3487322.